Universiteit Utrecht

MSc. Thesis in Theoretical Physics

Dynamics of structural defects in graphene

Author:
Li'ao Wang
3822176
Utrecht University

Supervisor:
Prof. Gerard T. Barkema
Institute for Theoretical Physics
Utrecht University

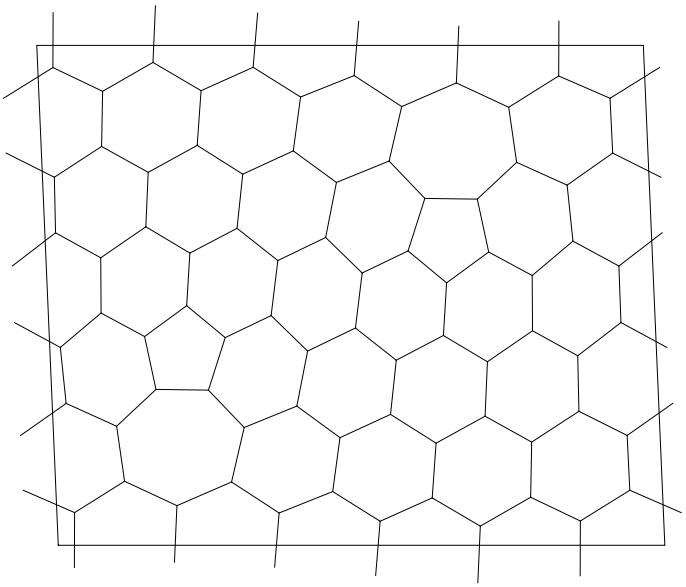

May 1, 2013

Abstract

Equilibrium and dynamical properties of structural defects in graphene are studied as function of temperature. The energetically favored structural defect is a Stone-Wales defect in an otherwise perfect hexagonal lattice. The two pentagon-heptagon pairs that form a Stone-Wales defect are able to move in one direction without affecting the total number of atoms in the system. The separation distance between defect pairs thus defines the state space of the system.

Calculation of equilibrium energies and deformation of a graphene sample yield logarithmic and linear dependence on the separation distance respectively. Equilibrium energies lead to three temperature regimes separated by two critical points.

Movement of defect pairs is modeled using an energy barrier between states. The mean square displacement is studied in these regimes through a stochastic model. At small timescales, this mean square displacement shows the expected diffusive behavior in all regimes. At large timescales however, anomalous (subdiffusive) behavior with a temperature dependent exponent is observed for high temperatures. For low temperatures, the mean square displacement converges to a constant. These two regimes are separated by a critical temperature at which the mean square displacement diverges logarithmically. Extrapolating Einstein-Smoluchowski to this system yields a shear deformation that increases to infinity but at a non-constant velocity that for low temperatures decreases to zero.

Contents

1 Introduction **3**

2 Structure of graphene **4**
2.1 Hamiltonian and ground state 4
2.2 Excited states from structural defects 5
2.2.1 Single defect 5
2.2.2 Multiple defects 6

3 Equilibrium energies and properties **10**
3.1 Energy and deformation 10
3.2 Equilibrium properties 12

4 Dynamics of structural defects **15**
4.1 Possible transitions and energy barriers 15
4.2 Stochastic modeling 16
4.3 Mean squared displacement 17
4.3.1 Small timescales 18
4.3.2 Large timescales 18

5 Discussion **22**
5.1 Extrapolating Einstein-Smoluchowski 22
5.2 Outlook 23

6 Conclusion **24**

1 Introduction

Graphene, as the first two-dimensional crystal to ever have been isolated [1], has been studied extensively. Over four hundred years after its invention it was finally spotted in 2004 [2]. Six years later, this research was rewarded the Nobel Prize in physics. Though it is a crystalline material, the second law of thermodynamics dictates some amount of disorder. The production of crystals also creates impurities and defects. These defects generally play a role in many characteristics of materials such as the conductivity of semiconductors and the mechanical strength of metals [3]. Defects in two dimensional crystals have only been considered recently, since it was long believed they could not exist due to the Mermin-Wagner theorem [4]. After graphene was isolated however, structural defects in graphene were also discovered and can even be induced deliberately. Several experimental studies have shown images of native or induced defects in graphene [5–8]. As in all materials, these defects affect conductivity, mechanical strength and optical properties of graphene. Understanding the behavior of these defects is key to understanding graphene.

In this thesis, the mechanical ground state of graphene is considered and a potential to describe it is introduced. Excitations of this potential in the form of structural defects are studied. Equilibrium properties of these excited states are computed and the dynamics of the system is modeled to explore the mechanics of graphene.

2 Structure of graphene

Graphene is a two-dimensional material consisting of only carbon atoms. The ground state electron configuration of carbon is $1s^2 2s^2 2p^2$. In the first excited state ($1s^2 2s 2p^3$), hybridization between the s orbital and two of the p orbitals creates three sp^2 hybrid orbitals that can form covalent bonds with other carbon atoms. These bonds arrange themselves to get as far apart as possible resulting in trigonal planar geometry: three identical bonds in one plane with 120° angles between them. Thus each carbon atom forms three bonds with the same bond length and all bond angles are 120°. The result is a regular hexagonal lattice. The bond length within graphene is approximately 0.142nm.

The remaining electrons of the unaffected p orbitals (one per carbon atom) are delocalized over the entire structure.

2.1 Hamiltonian and ground state

To describe graphene, a Hamiltonian is needed that yields the according ground state and that is computable for large systems. Ignoring long range interactions between atoms, the interactions between atoms close to one another define the geometry of the lattice. This geometry depends on the length of the bonds and the angles between them so the relevant energies are those needed to stretch and to bend bonds. A potential that is computable and describes these energies is the Keating potential [9]:

$$H = \frac{3}{16}\frac{\alpha_K}{d^2}\sum_{<i,j>}(|\mathbf{r}_{ij}|^2 - d^2)^2 + \frac{3}{8}\frac{\beta_K}{d^2}\sum_{<i,j,k>}(\mathbf{r}_{ij}\cdot\mathbf{r}_{ik} + \frac{d^2}{2})^2. \tag{1}$$

Here the first sum runs over all atoms i and j that are connected through a bond represented by the vector $\mathbf{r}_{ij}$. The second sum runs over all atoms i, j and k for which bonds $\mathbf{r}_{ij}$ and $\mathbf{r}_{ik}$ share an atom.

The first term represents the energy needed to stretch (or compress) a bond beyond its natural unconstrained bond length d. The second term represents the energy needed to bend a pair of bonds from the natural unconstrained bond angle (120°). Though the bond length in graphene is known, the values of the stretching force constant α_K and the bending force constant β_K are not. Therefore the values as known from fits for amorphous silicon are used: $d = 2.35$Å, $\alpha_K = 2.965$ eV Å^{-2} [10] and $\beta_K = 0.285\alpha$ [11]. The value chosen for d merely sets the length scale of the system. The values of α_K and β_K lead to qualitatively similar results as long as their ratio is such that the variation of the bond lengths from d is small compared to the value of d itself. The approach is similar to the one used in [12].

Eq. (1) vanishes when $|\mathbf{r}_{ij}|^2 = d^2$ and $\mathbf{r}_{ij}\cdot\mathbf{r}_{ik} = -\frac{d^2}{2}$ for all bonds. Thus the graphene lattice with bond lengths d and bond angles of 120° is indeed the ground state of this Hamiltonian. Such a regular hexagonal lattice is shown in figure 1. This figure also illustrates the two directions that can be distinguished within graphene: the zigzag direction and the armchair direction. The system is symmetric under rotations of 60°.

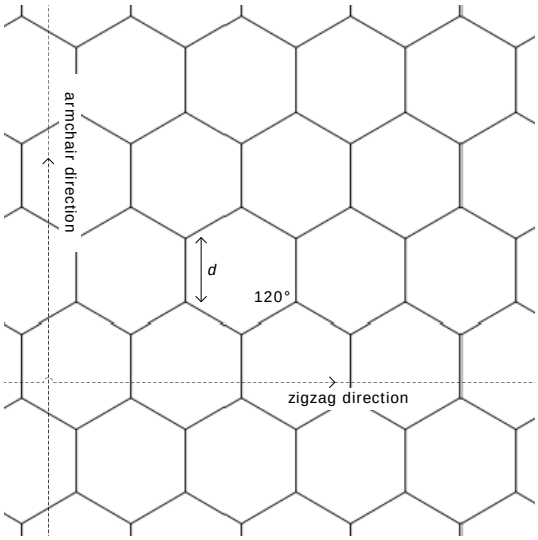

Figure 1: Schematic graphene sample consisting of regular hexagons with bond length d. The zigzag and armchair directions can be distinguished and the system is symmetric under rotations of 60°.

2.2 Excited states from structural defects

Irregularities in the hexagonal lattice form excited states of the Hamiltonian in eq. (1). Only defects that satisfy the following two conditions are considered:

i *The total number of atoms is invariant.*
Interstitial atoms, vacancies or impurities do not preserve the number of atoms and are therefore not suitable defects.

ii *The energy of every state must be finite.*
For when the energy of a state increases to infinity, the Boltzmann probability to be in this state decreases to zero.

A defect that preserves the number of atoms is a pentagon-heptagon pair as shown in figure 2. The pentagon and the heptagon together have the same amount of atoms as there are in two hexagons. A first possible candidate for an excited state is thus a perfect lattice with a single pentagon-heptagon pair.

2.2.1 Single defect

Figures 2a and 2b show the Burger's vector **b** of the dislocation caused by a pentagon-heptagon pair. As can be seen in figure 2c, this is an edge dislocation: an extra row is inserted due to the defect. According to elasticity theory the energy of an edge dislocation is proportional to the logarithm of the crystal size [3]

$$E_e = \frac{Gb^2}{4\pi(1-\nu)} \ln \frac{R}{r_0}, \tag{2}$$

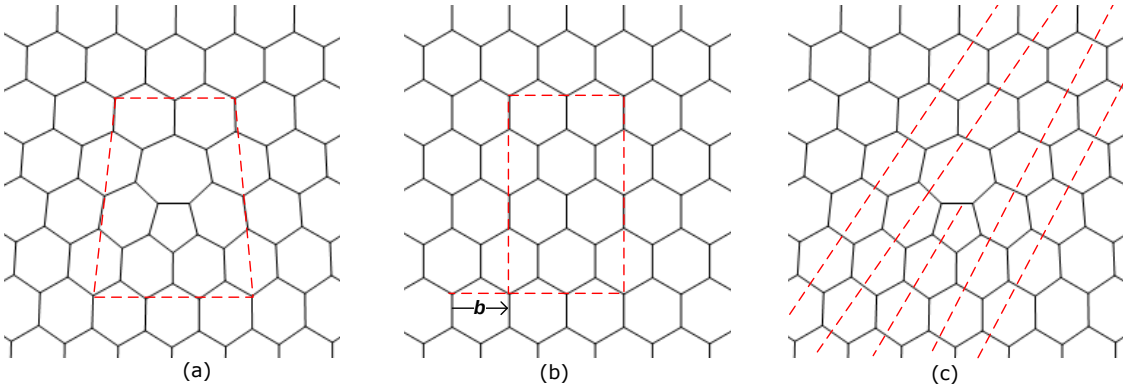

Figure 2: Graphene sample with a closed loop drawn around a single pentagon-heptagon pair (a) and the same closed loop drawn on a perfect hexagonal lattice (b). The difference between the two loops is the Burger's vector of the defect. This type of defect causes the addition of an extra row starting at the defect (c).

with G the shear modulus of the material, ν its Poisson ratio, r_0 the radius at which elasticity theory breaks down (roughly $5b$) and $b = |\mathbf{b}|$ the magnitude of the Burger's vector of the dislocation. The system size is indicated by R, so eq. (2) shows that the energy of a pentagon-heptagon pair increases to infinity for infinite systems. Thus, according to condition (**ii**), a single defect consisting of a pentagon-heptagon pair cannot exist by itself.

However several of these defects can exist at finite energies. The strain fields of multiple defects cancel when their Burger's vectors add up to zero. Possible configurations are thus a pair of defects and a triplet of defects with canceling Burger's vectors.

2.2.2 Multiple defects

Multiple defects with canceling Burger's vectors are shown in figures 3 and 4:

i *a Stone-Wales defect* preserves the number of atoms (3b),

ii *an inverse Stone-Wales defect* requires the addition of two atoms (3d),

iii *a triplet with pentagons on the outside* lacks two atoms (4b),

iv *a triplet with heptagons on the outside* requires the addition of four atoms (4c).

A possible first excited state of a system with the regular hexagonal lattice as its ground state thus becomes a Stone-Wales defect in an otherwise perfect lattice. The two pentagon-heptagon pairs can be next to one another as in the case of a Stone-Wales defect but they can also be further apart. Figure 5 shows two defects with nonzero distances between them in both the armchair (Δ_a) and the zigzag (Δ_z) directions. It also illustrates how these distances are defined relative to the lattice. Each increase with $\frac{1}{2}$ of Δ_a however, requires the addition of two extra atoms. So when starting in a state with a pair of defects separated by some distance in the armchair direction, any state that changes Δ_a is not a suitable excitation because it violates condition (**i**). To conclude:

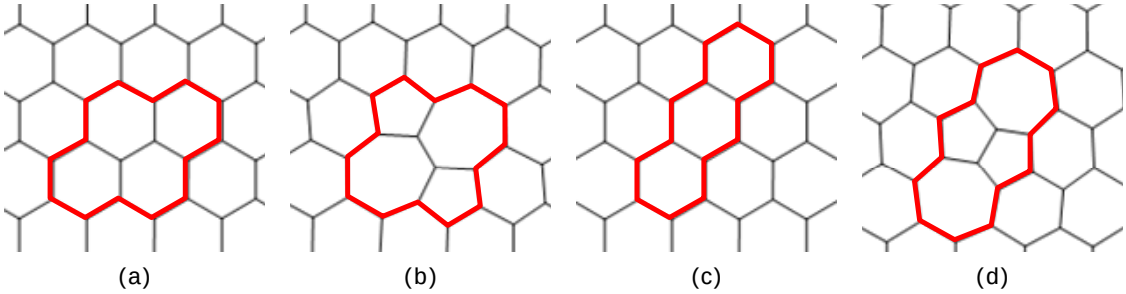

Figure 3: Atoms and bonds that are deformed locally by the insertion of a defect on a regular hexagonal lattice (a) and on a lattice with a Stone-Wales defect (b) show that this preserves the number of atoms. The same is illustrated for an inverse Stone-Wales lattice (c,d) showing that this requires the addition of two atoms.

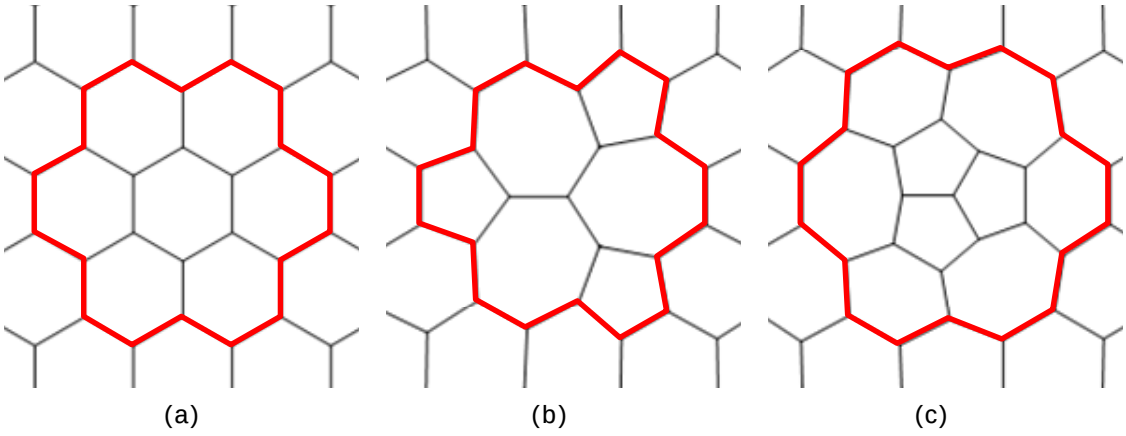

Figure 4: Atoms and bonds that are deformed locally by the insertion of a triplet on a regular lattice (a), on a lattice with a triplet with the pentagons on the outside (b) and on a lattice with a triplet with the heptagons on the outside (c). In the case of the pentagons on the outside, the defect lacks two atoms and in the case of the heptagons on the outside the defect requires the addition of four atoms.

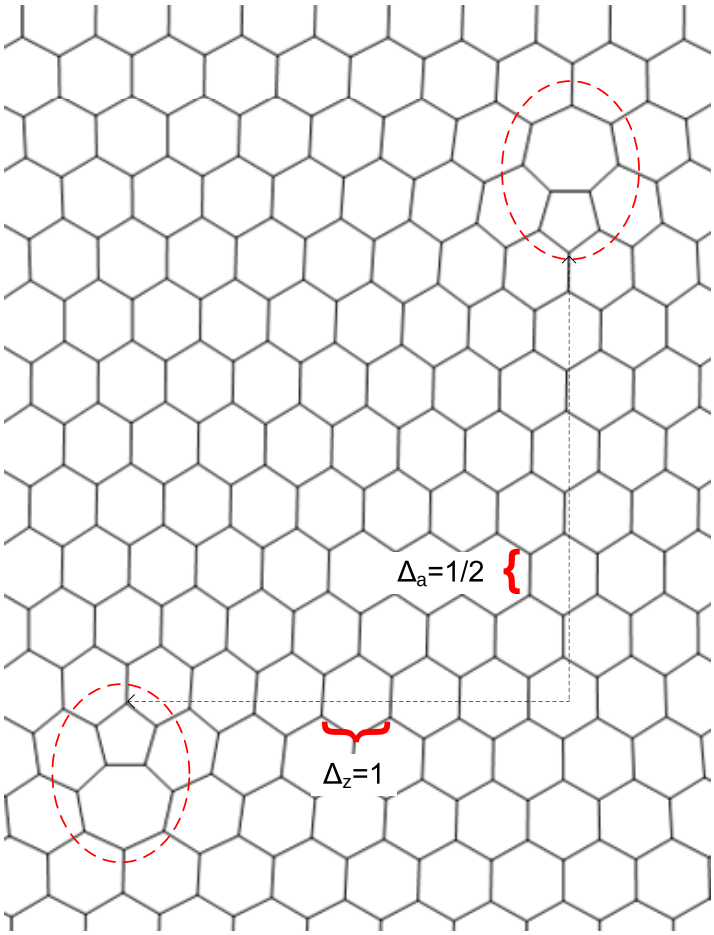

Figure 5: Defect pair separated in both the zigzag and armchair directions. In terms of the lattice, the values for both separations are $\Delta_z = 6$ and $\Delta_a = 4$. Change in Δ_z preserves the number of atoms while each increase with $\frac{1}{2}$ of Δ_a requires the addition of two atoms.

- A pair of defects arranged like a Stone-Wales defect has canceling Burger's vectors and preserves the number of atoms.
- The two defects of this pair can be separated in both the zigzag and the armchair directions, however due to invariance of the total number of atoms the separation in the armchair direction must remain the same: defects cannot move in the armchair direction. Movement in the zigzag direction is possible without changing the total number of atoms.
- States with pairs that are not separated in the armchair direction are suitable excited states of the ground state since they preserve the total number of atoms in the ground state.

Each system is now characterized by its size L and the separation in the armchair direction between two defects Δ_a. These values remain the same for each state the system is in (e.g. a

system wherein the defects have some nonzero Δ_a cannot transition into the ground state). The state space of a system of size L with armchair separation distance Δ_a is then defined by the value of Δ_z. This separation distance takes values $0, 1, \cdots, L-2$ yielding $L-1$ distinct possible states. Knowing the state space, equilibrium energies and properties can now be studied.

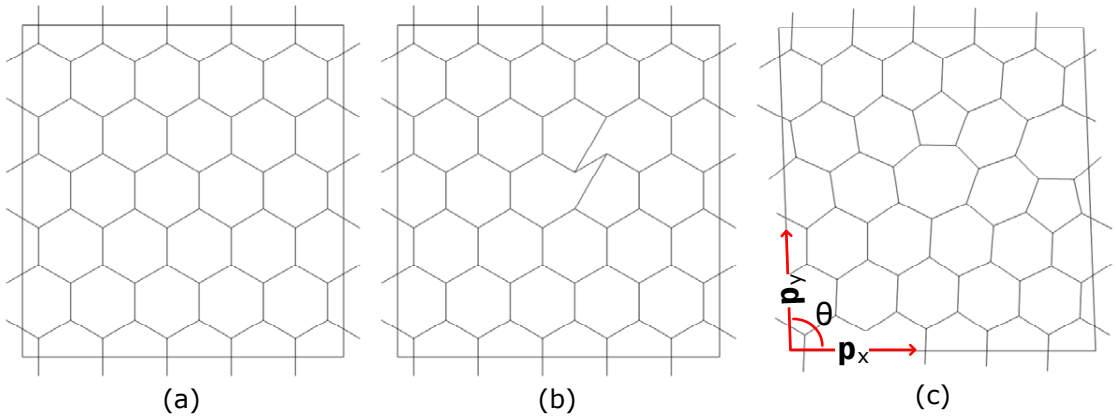

Figure 6: Periodic graphene lattice sample as it undergoes the three steps that lead to a relaxed configuration with a defect: a perfect hexagonal lattice is generated (a), bonds are rearranged to create the topology of a defect (b) and the system is relaxed according to the hamiltonian of eq. (1) (c). In the final relaxed configuration, the angle θ between the periodic axes of the sample has changed.

3 Equilibrium energies and properties

The excited states of interest are regular hexagonal lattices with a defect pair. The Burger's vectors of the defects must cancel and the pair can have various separation values along the Δ_z direction. These configurations of the lattice are created as follows:

1) a regular hexagonal lattice of size L is generated,

2) bonds are rearranged to create the topology of a state,

3) the system is relaxed by minimizing the hamiltonian of eq. (1) using the conjugate gradient method.

Figure 6 shows the lattice as it undergoes the three steps. The sample is modeled with periodic boundary conditions, so the location of the defect pair does not matter, only its separation in the Δ_z direction.

3.1 Energy and deformation

The energy of the relaxed system is determined using the Keating potential of eq. (1). The presence of a defect pair not only increases the equilibrium energy of the system but also deforms the lattice. As shown in figure 6c the angle θ between the periodic axes $\mathbf{p}_x$ and $\mathbf{p}_y$ of the sample is influenced by the defects. Figures 7 and 8 show the minimized energies of the states and the deformation of the sample for various lattice sizes.

The equilibrium energy is calculated to increase logarithmically with the separation. Apart from finite size effects when $\Delta_z \approx L$ the energy yields the same function of Δ_z for all system sizes. The deformation is dependent on both system size and defect separation. These

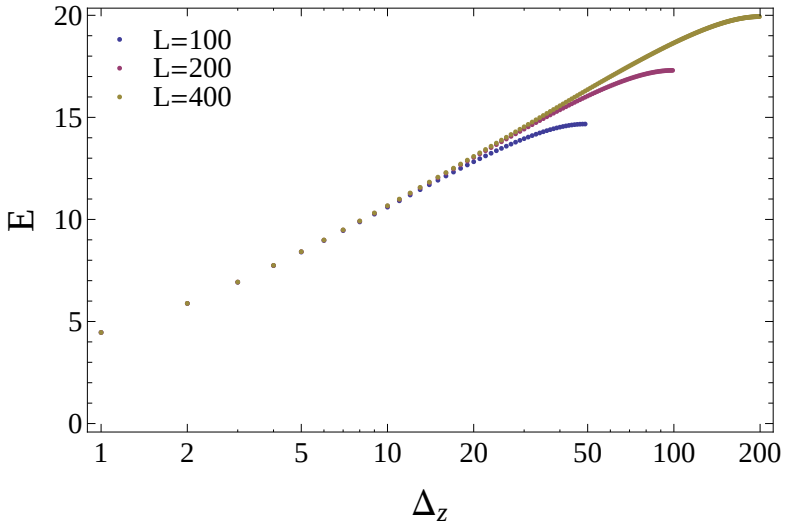

Figure 7: Energy of the relaxed system with a defect pair separated in the Δ_z direction: $\Delta_z = 0, 1, \cdots, L/2$ (due to periodicity larger values of Δ_z give no new information, the energy is symmetric) for various lattice sizes. The plot shows that $E \propto \log \Delta_z$.

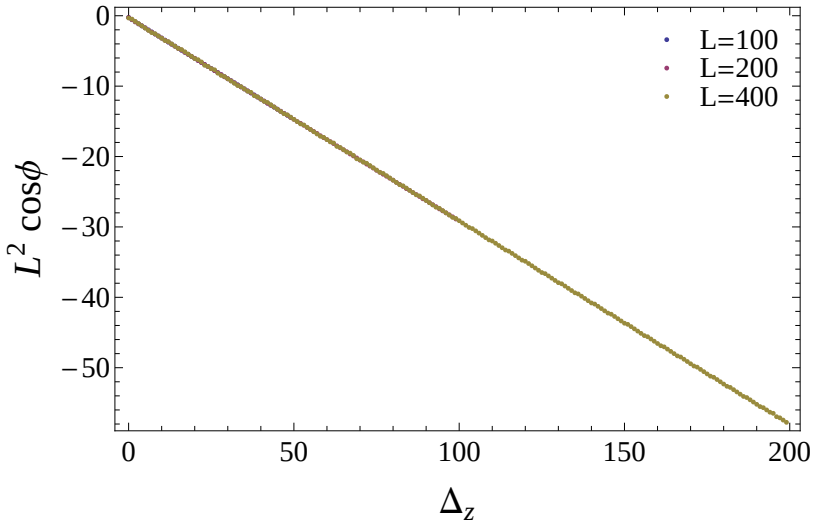

Figure 8: Deformation due to a defect pair separated in the Δ_z direction for various lattice sizes. The data collapses for different values of L. This indicates that $L^2 \cos\theta \propto \Delta_z$.

simulations thus lead to the following results for the energy and deformation:

$$\begin{aligned} E(\Delta_z) &= E_0 + \alpha \ln(\Delta_z + 1), \\ L^2 \cos\theta &\propto \Delta_z. \end{aligned} \tag{3}$$

This parametrization of the energy is chosen so that $E(0) = E_0$ is the energy for a system with a Stone-Wales defect after relaxation. The measured values for E_0 and α are 1.80 eV and 3.69 eV respectively. Expansion of the second equation near $\theta = 90°$, since angle fluctuations will be small, leads to the linear relation

$$\theta \propto \Delta_z. \tag{4}$$

3.2 Equilibrium properties

Now that the energy and deformation dependencies on the separation distance Δ_z are known, equilibrium properties can be calculated for a system with $L \to \infty$. The partition function is first examined, this is the sum over all possible states weighted with their energy:

$$\begin{aligned} Z(\beta) &= \sum_{\Delta_z=0}^{\infty} e^{-\beta E(\Delta_z)} \\ &= \sum e^{-\beta\Big(E_0 + \alpha \ln(\Delta_z+1)\Big)} \\ &= e^{-\beta E_0} \sum (\Delta_z + 1)^{-\alpha\beta} \\ &= e^{-\beta E_0} \zeta(\alpha\beta) \qquad \text{for } \beta > \frac{1}{\alpha}, \end{aligned} \tag{5}$$

with ζ the Riemann zeta function. For $\beta \leq \frac{1}{\alpha}$ the sum diverges and thus the partition function is not well defined. Next, using the partition function the mean separation distance $\langle \Delta_z \rangle$ is calculated:

$$\begin{aligned} \langle \Delta_z \rangle(\beta) &= \frac{1}{Z} \sum_{\Delta_z=0}^{\infty} \Delta_z e^{-\beta E(\Delta_z)} \\ &= \frac{1}{\zeta(\alpha\beta)} \sum \Delta_z (\Delta_z + 1)^{-\alpha\beta} \\ &\overset{\beta > \frac{2}{\alpha}}{\approx} \int_0^{\infty} dx\, x(x+1)^{-\alpha\beta} \\ &= \frac{1}{\zeta(\alpha\beta)} \frac{1}{(1-\alpha\beta)(2-\alpha\beta)} \qquad \text{for } \beta > \frac{2}{\alpha}. \end{aligned} \tag{6}$$

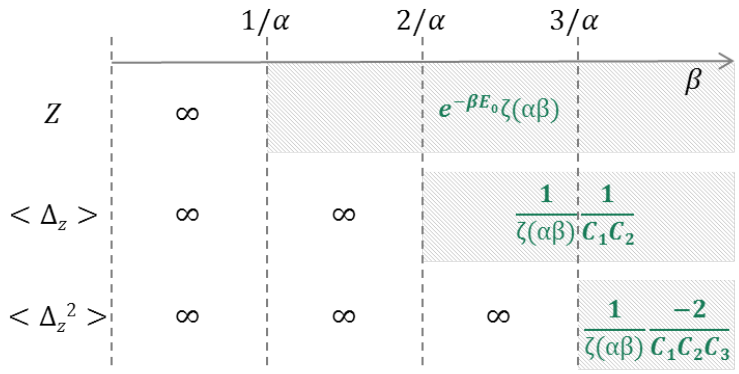

Figure 9: The system has three temperature regions where the partition function converges: for $\frac{1}{\alpha} < \beta < \frac{2}{\alpha}$ both the means of the quadratic and non-quadratic separations diverge, for $\frac{2}{\alpha} < \beta < \frac{3}{\alpha}$ the mean separation converges but the mean quadratic separation diverges and for $\beta > \frac{3}{\alpha}$ both converge. The values to which the sums converge (when applicable) are shown in the figure, with $C_i = \frac{1}{i-\alpha\beta}$ and ζ the Riemann zeta function.

This sum converges to the integral for $\beta > \frac{2}{\alpha}$ and diverges for smaller β. Similarly, the mean quadratic separation becomes

$$\begin{aligned}
\langle \Delta_z^2 \rangle(\beta) &= \frac{1}{Z} \sum_{\Delta_z=0}^{\infty} \Delta_z^2 e^{-\beta E(\Delta_z)} \\
&= \frac{1}{\zeta(\alpha\beta)} \sum \Delta_z^2 (\Delta_z + 1)^{-\alpha\beta} \\
&\overset{\beta > \frac{3}{\alpha}}{\approx} \int_0^{\infty} dx\, x^2 (x+1)^{-\alpha\beta} \\
&= \frac{1}{\zeta(\alpha\beta)} \frac{-2}{(1-\alpha\beta)(2-\alpha\beta)(3-\alpha\beta)} \qquad \text{for } \beta > \frac{3}{\alpha}
\end{aligned} \tag{7}$$

for $\beta > \frac{3}{\alpha}$ where the sum converges to the integral. For higher temperatures the mean quadratic separation diverges.

Thus, in the region where the system has a well defined partition function, there are three regimes separated by two critical points as illustrated in figure 9.

I. For $\frac{1}{\alpha} < \beta < \frac{2}{\alpha}$ both the mean separation and the mean quadratic separation diverge. At these high temperatures two defects eventually move infinitely far away from one another.

II. For $\frac{2}{\alpha} < \beta < \frac{3}{\alpha}$ the mean separation converges but the mean quadratic separation diverges - the logarithmic potential causes a Boltzmann probability function with a densely populated tail. This tail, containing the states with high energies and large separations, dominates the mean *quadratic* separation but not the mean separation.

III. For $\beta > \frac{3}{\alpha}$ both the means of the quadratic and non-quadratic separations converge. In this third regime the defects stay within finite distance of one another.

These regions can be studied by modeling the dynamics of the system as a stochastic process. Using the mean square displacement of the separation distance, the behavior of the system can be characterized near its critical points.

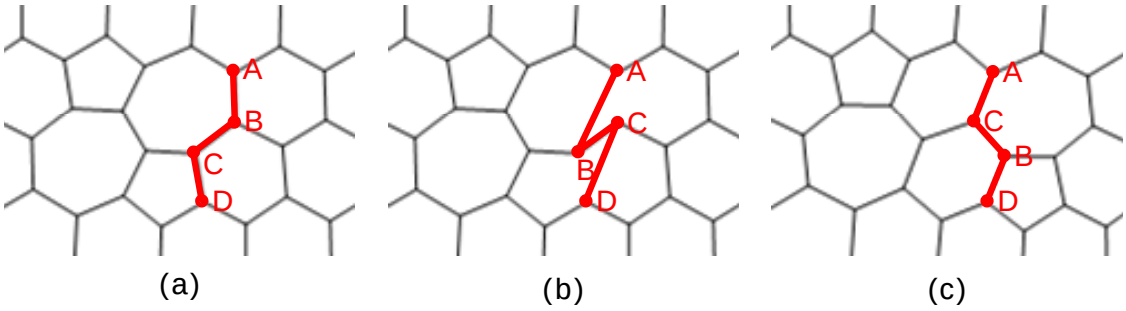

Figure 10: The outer atoms and bonds of a defect are involved in movement (a), the bonds of these atoms rearrange to create the new topology (b) and the atom positions and bond lengths relax into the optimal configuration (c).

4 Dynamics of structural defects

To model the dynamics of the system, transitions between states must be considered. In this case, transitions equal movement of a defect along the zigzag direction. This movement is illustrated in figure 10.

4.1 Possible transitions and energy barriers

The figure shows that the defects move one lattice step at the time, and that two things must happen in order for a defect to move: **i**) bonds need to rearrange and **ii**) bond lengths and atom positions need to relax into the configuration with minimal energy for the new state. The first observation implies that for $0 < \Delta_z < L - 2$ the only possible transitions are:

$$\Delta_z \to \Delta_z \pm 1.$$

For $\Delta_z = 0$ the only possible transition is to $\Delta_z = 1$ and for $\Delta_z = L - 2$ the only possible transition is to $\Delta_z = L - 3$.

The second observation implies that a transition requires bonds to break and reattach, and atoms to reposition. How rearrangement of bonds and movement of atoms happen exactly and the order in which the two happen is not known. It is clear however, that this causes some temporary suboptimal energy in between equilibrium states. This is modeled by an energy barrier between two consecutive minima as shown in figure 11. These barriers are assumed to

- **o** lie halfway between one energy minimum and the next,
- **o** differ from the minima by a constant E_1.

The height of the barrier is thus approximated by

$$E_{max}(\Delta_z, \Delta_z \pm 1) = \frac{E(\Delta_z \pm 1) + E(\Delta_z)}{2} + E_1,$$

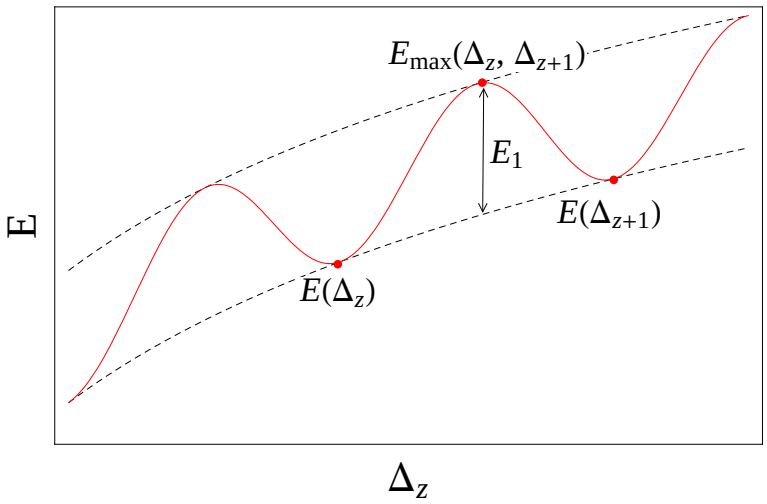

Figure 11: The system must cross an energy barrier to transition from one relaxed state to the next. This barrier is caused by the rearrangement of bonds and repositioning of atoms that are necessary for defect movement (schematic representation).

and the energy needed to cross a barrier and transition to another state becomes

$$\Delta E(\Delta_z, \Delta_z \pm 1) = \frac{E(\Delta_z \pm 1) - E(\Delta_z)}{2} + E_1. \tag{8}$$

4.2 Stochastic modeling

The transition energies of eq. (8) are used to model the transitions as a stochastic process [13]:

- when the system is in state $\Delta_z = i$, it can move either to state $\Delta_z = i+1$ or $\Delta_z = i-1$,
- the time between two consecutive events is exponentially distributed,
- the rates at which the separation increases or decreases are given by $\lambda_i = 2e^{-\beta\Delta E(i,i+1)}$ and $\mu_i = 2e^{-\beta\Delta E(i,i-1)}$ respectively, $\mu_0 = 0$ since the separation distance cannot become smaller than zero (annihilation of a defect pair is not considered in this process) and in the finite size case also $\lambda_{L-2} = 0$ (as are all higher λ's and μ's) since Δ_z must fit on the lattice.

The factor 2 in the rates is caused by the fact that there are two ways to move from one state to another: both defects can move to create the new state. These rates can be interpreted as the expected number of events per time unit. The instantaneous probabilities to move from state i to state j in infinitesimal time dt thus become:

$$p_{ij}(dt) = \begin{cases} \lambda_i dt & j = i+1 \\ \mu_i dt & j = i-1 \\ 1 - \lambda_i dt - \mu_i dt & j = i \end{cases} \tag{9}$$

In matrix form this can be written as $\mathbf{p}(dt) = \mathbf{1} + \mathbf{Q}dt$ with $\mathbf{Q}$ the following matrix:

$$\mathbf{Q} = \begin{pmatrix} -\lambda_0 & \lambda_0 & 0 & 0 & \cdots \\ \mu_1 & -(\lambda_1+\mu_1) & \lambda_1 & 0 & \cdots \\ 0 & \mu_2 & -(\lambda_2+\mu_2) & \lambda_2 & \cdots \\ 0 & 0 & \mu_3 & -(\lambda_3+\mu_3) & \cdots \\ \vdots & \vdots & \vdots & \vdots & \ddots \end{pmatrix}.$$

Now for each time t the probabilities to move from state i to state j in time $t+dt$ are obtained by multiplying the probability to move from i to some state k in time dt with the probability to move from this state k to state j in the remaining time t: $p_{ij}(t+dt) = \sum_k p_{ik}(dt)p_{kj}(t)$. In matrix form:

$$\begin{aligned} \mathbf{p}(t+dt) &= \mathbf{p}(dt)\mathbf{p}(t) \\ &= (\mathbf{1} + \mathbf{Q}dt)\mathbf{p}(t) \\ &= \mathbf{p}(t) + \mathbf{Q}\mathbf{p}(t)dt. \end{aligned}$$

This can be rearranged into a differential equation

$$\mathbf{p}'(t) = \frac{\mathbf{p}(t+dt) - \mathbf{p}(t)}{dt} = \mathbf{Q}\mathbf{p}(t)$$

which is solved by an exponential solution:

$$\mathbf{p}(t) = e^{\mathbf{Q}t}$$

with boundary conditions $\mathbf{p}(0) = \mathbf{1}$, since it takes some finite time before a transition occurs. Now $\mathbf{Q}$ can be decomposed into matrices $\mathbf{U}$ and $\mathbf{D}$, with $\mathbf{D}$ the matrix with the eigenvalues of $\mathbf{Q}$ on its diagonal leading to a simpler form of the solution:

$$\mathbf{p}(t) = \mathbf{U}e^{\mathbf{D}t}\mathbf{U}^{-1}. \tag{10}$$

The entries of this matrix can now be computed for all states i and j and for all times t. For all times t it becomes possible to determine the probability that the system has moved from state i to state j in this time. This matrix contains the necessary information to describe the dynamics of the system.

4.3 Mean squared displacement

A quantity that describes the dynamics of the system is the mean squared displacement of the separation as a function of time:

$$\begin{aligned} \langle \Delta_z^2 \rangle(t) &= \left\langle \Big(\Delta_z(t) - \Delta_z(0) \Big)^2 \right\rangle \\ &= \sum_{i=0}^{\infty} B_i \sum_{j=0}^{\infty} (j-i)^2 p_{ij}(t), \end{aligned} \tag{11}$$

with B_i the Boltzmann probability to be in state i. The limit for large timescales becomes

$$\begin{aligned} \langle \Delta_z^2 \rangle(t) &= \langle \Delta_z(t)^2 \rangle + \langle \Delta_z(0)^2 \rangle - 2\langle \Delta_z(t)\Delta_z(0) \rangle \\ &\overset{t\to\infty}{\to} 2\Big(\langle \Delta_z^2 \rangle - \langle \Delta_z \rangle^2 \Big) \\ &= 2\mathrm{Var}(x). \end{aligned} \tag{12}$$

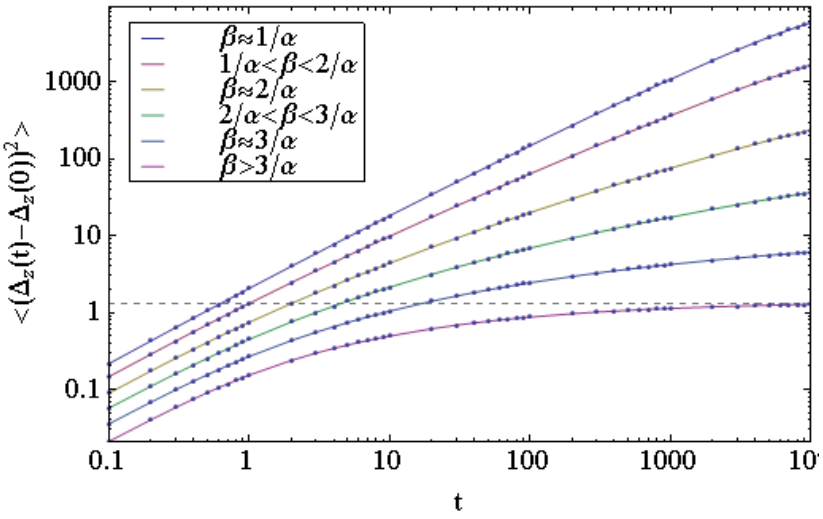

Figure 12: The mean squared displacement for various temperatures plotted on a log-log scale shows that for high temperatures the mean squared displacement behaves as a power-law with temperature dependent exponent. The displacement converges to the expected constant of eq. (12) (dashed line) for low temperatures.

Recalling eq. (6) and eq. (7) it becomes clear that this limit only exists for $\beta > 3/a$. Now using eq. (11) the evolution of the mean squared displacement in time can be determined and eq. (12) yields the limit (if it exists) for long timescales.

Figures 12 and 13 show the mean squared displacement in time on a log-log scale and a lin-log scale respectively, in the various temperature regimes. The log-log plot indicates that for high temperatures, the mean squared displacement behaves like a power-law with a temperature dependent exponent. In both plots it can be seen that for low temperatures the mean squared displacement converges to a constant, as was predicted by eq. (12). The lin-log plot shows that at the critical point $\beta = \frac{3}{\alpha}$ the mean squared displacement diverges logarithmically.

4.3.1 Small timescales

Zooming in on small timescales, figure 14 shows that the mean squared displacement is linear in time for all temperatures. Thus for all temperatures, the system exhibits diffusive behavior for small t. In a small time dt, a defect can either take a step, or not take a step. The probability to take a step in time dt is linear in time (recall eq. (9)) thus so is the mean squared displacement.

4.3.2 Large timescales

Figures 15 and 16 show the mean squared separation for high temperatures on a log-log scale and for low temperatures on a lin-log scale. Looking at the first plot, it becomes clear that

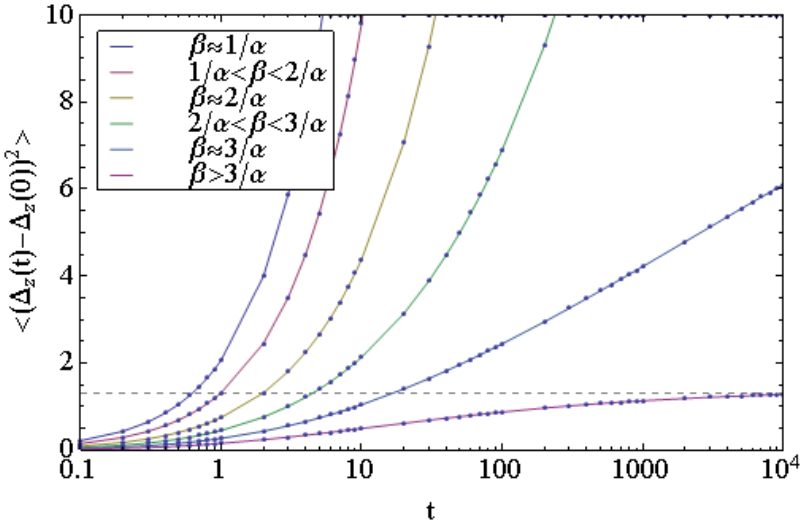

Figure 13: The mean squared displacement for various temperatures plotted on a lin-log scale shows that for $\beta = \frac{3}{\alpha}$ it diverges logarithmically. This plot too shows that the displacement converges to the expected constant of eq. (12) (dashed line) for low temperatures.

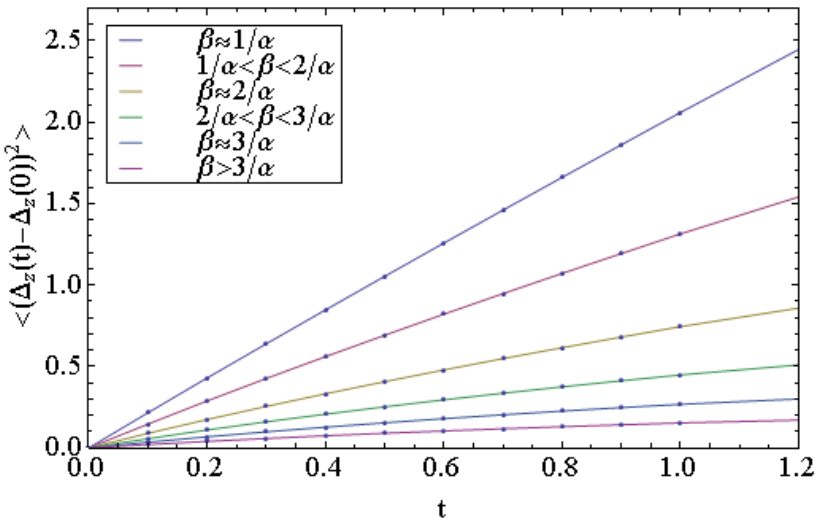

Figure 14: The mean squared displacement for small timescales shows linear behavior in time at all temperatures. The system exhibits the expected diffusive behavior.

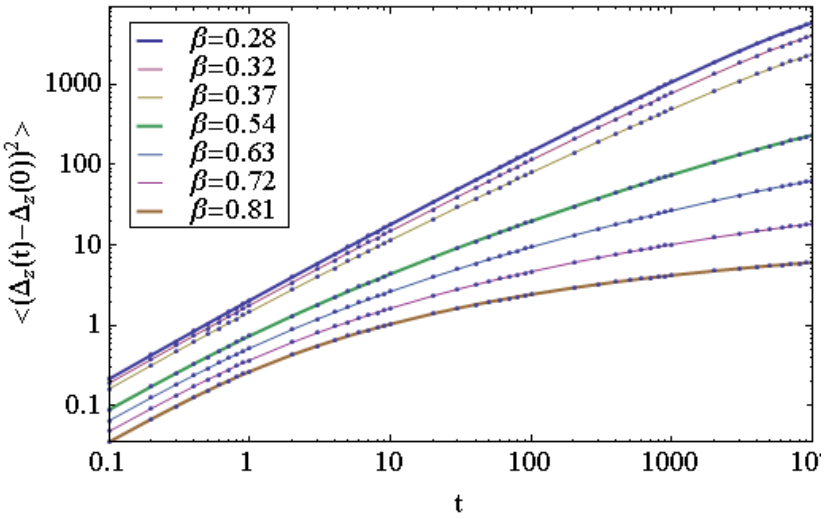

Figure 15: For large timescales and high temperatures the mean squared displacement is plotted on a log-log scale. The thick lines show the mean squared displacement at the three critical points $\beta = \frac{1}{\alpha}, \beta = \frac{2}{\alpha}$ and $\beta = \frac{3}{\alpha}$. Around the first critical point, the mean squared displacement shows subdiffusive behavior (power-law with an exponent smaller than one). The exponent is temperature dependent and decreases as β increases.

for $\frac{1}{\alpha} < \beta < \frac{2}{\alpha}$ the system is subdiffusive:

$$\left\langle \Big(\Delta_z(t) - \Delta_z(0)\Big)^2 \right\rangle \propto t^{\epsilon(\beta)}, \tag{13}$$

with $\epsilon(\beta) < 1$. This exponent becomes smaller as the temperature decreases until at $\beta = \frac{3}{\alpha}$ it becomes zero and a logarithm is left:

$$\left\langle \Big(\Delta_z(t) - \Delta_z(0)\Big)^2 \right\rangle \propto \log(t). \tag{14}$$

For $\beta > \frac{3}{\alpha}$ the mean squared displacement converges to a known constant as expected:

$$\begin{aligned}\left\langle \Big(\Delta_z(t) - \Delta_z(0)\Big)^2 \right\rangle &\propto 2\Big(\langle \Delta_z^2 \rangle - \langle \Delta_z \rangle^2\Big) \\ &= \frac{2}{\zeta(\alpha\beta)} \left\{ \frac{-2}{(1-\alpha\beta)(2-\alpha\beta)(3-\alpha\beta)} - \frac{1}{\zeta(\alpha\beta)} \left(\frac{1}{(1-\alpha\beta)(2-\alpha\beta)} \right)^2 \right\}.\end{aligned} \tag{15}$$

The mean squared displacement is a measure for the natural fluctuations in a system. The next step is to connect these natural fluctuations to a system's reaction to a small force.

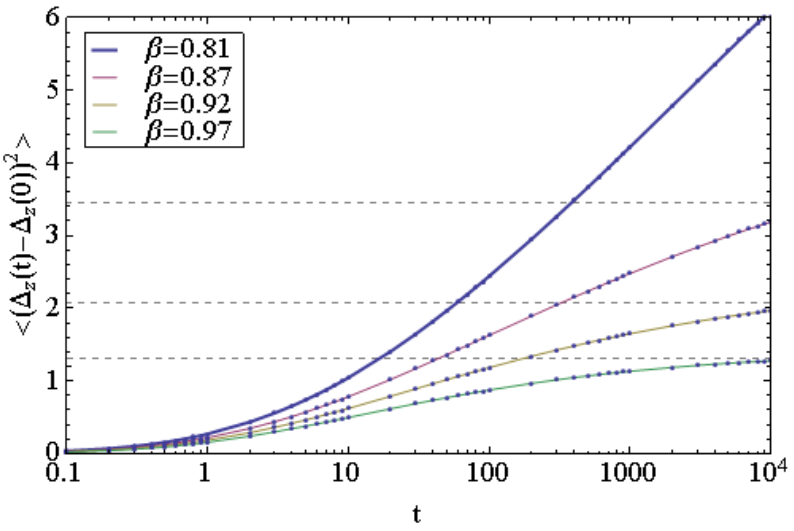

Figure 16: For large timescales and low temperatures the mean squared displacement is plotted on a lin-log scale. Again the thick line represents the mean squared displacement at the critical point $\beta = \frac{3}{\alpha}$. At this temperature the exponent has decreased to zero, leaving a logarithm. At higher temperatures the mean squared displacement converges to the expected values (dashed lines).

5 Discussion

In 1905 Albert Einstein wrote a paper on Brownian motion in which he connected diffusion for Brownian particles with their mobility (i.e. the ratio of a particle's velocity to an applied force) [14]. One year later Marian Smoluchowski found the same relationship independently of Einstein [15]. What they discovered was an early version of the fluctuation-dissipation theorem.

5.1 Extrapolating Einstein-Smoluchowski

The first part of the argument yields the distance a Brownian particle travels on average in some time t by solving the diffusion equation. This results in a mean squared displacement of

$$\left\langle \Big(\mathbf{r}(t) - \mathbf{r}(0)\Big)^2 \right\rangle = 2dDt,$$

with d the dimensionality of the system (in this case $d = 1$ since the defects can move only in one direction) and D the diffusion constant. Then, after applying a small force f and waiting for a new equilibrium to establish, fluxes due to drift (i.e. due to the applied force) and diffusion are required to add up to zero since there is no net flow of particles in equilibrium. This results in the following relation between the diffusion constant and velocity v in reaction to an applied force:

$$D = \frac{v}{f} k_B T,$$

with k_B the Boltzmann constant, i.e. $k_B T = \frac{1}{\beta}$. Combining these two equations, a relation for the particle velocity caused by an applied force is obtained in terms of the mean squared displacement:

$$v = \beta f D = \beta f \frac{\left\langle \Big(\mathbf{r}(t) - \mathbf{r}(0)\Big)^2 \right\rangle}{2dt}. \tag{16}$$

Now this relationship holds for Brownian particles but the defects in this system are not Brownian particles. However in other research, extrapolating Einstein-Smoluchowski has proved successful even for non-Brownian particles [16]. To do this, recall eq. (13), eq. (14) and eq. (15). For large timescales the mean squared displacement of the separation distance between particles becomes

$$\left\langle \Big(\Delta_z(t) - \Delta_z(0)\Big)^2 \right\rangle \overset{t\to\infty}{\propto} \begin{cases} t^{\epsilon(\beta)} & \text{for } \beta < \frac{3}{\alpha} \\ \log(t) & \text{for } \beta = \frac{3}{\alpha} \\ \text{constant} & \text{for } \beta > \frac{3}{\alpha} \end{cases}. \tag{17}$$

Of interest however, is not the velocity of the defects in reaction to an applied force, but what this does to a graphene sample. Since it is known from eq. (4) that the deformation angle θ and the defect separation distance Δ_z are linearly related, it is possible to link the movement of defects to the sample deformation. The deformation angle describes how particles that were above each other in the sample prior to the deformation, have shifted in the zigzag direction after the deformation: it is the shear γ of the system. The force that causes shear is stress. Thus a relationship is found for the shear velocity $\dot{\gamma}$ as a reaction to a small applied stress σ

by plugging eq. (17) into eq. (16):

$$\dot{\gamma}(t) \overset{t\to\infty}{\propto} \begin{cases} \beta\sigma t^{\epsilon(\beta)-1} & \overset{t\to\infty}{\to} \infty & \text{for } \beta < \frac{3}{\alpha} \\ \beta\sigma \frac{\log(t)}{t} & \overset{t\to\infty}{\to} 0 & \text{for } \beta = \frac{3}{\alpha} \\ \frac{\beta\sigma}{t} & \overset{t\to\infty}{\to} 0 & \text{for } \beta > \frac{3}{\alpha} \end{cases} . \tag{18}$$

Integration yields the shear deformation in time as a reaction to the small applied stress σ:

$$\gamma(t) \overset{t\to\infty}{\propto} \begin{cases} \beta\sigma t^{\epsilon(\beta)} & \overset{t\to\infty}{\to} \infty & \text{for } \beta < \frac{3}{\alpha} \\ \beta\sigma \log(t)^2 & \overset{t\to\infty}{\to} \infty & \text{for } \beta = \frac{3}{\alpha} \\ \beta\sigma \log(t) & \overset{t\to\infty}{\to} \infty & \text{for } \beta > \frac{3}{\alpha} \end{cases} . \tag{19}$$

Now assume that even though graphene may have multiple defect pairs, these defect pairs do not influence each other. The total shear in the system is then the sum of the shear effects of the individual pairs. These equations thus indicate that when applying a small stress to graphene, it will deform infinitely but at a non-constant velocity that for low temperatures eventually becomes zero. For all temperatures with $\beta \geq \frac{3}{\alpha}$ the shear deformation of graphene will increase to infinity but it will deform slower and slower, until the shear velocity eventually decreases to zero.

5.2 Outlook

The model developed here studies moving defect pairs in graphene. Annihilation of defects is not considered in the dynamics, this can be understood as studying defects that have some separation in the armchair direction and can thus never annihilate. In reality however, defect pairs can be created and annihilated, and pairs can also interact with other pairs (e.g. a defect of one pair can annihilate with a defect of a different pair). These effects have not been considered so far.

Another note to be made is that the dynamics of the system are modeled as a stochastic process. A different common approach would be using Monte Carlo simulations to observe how the system behaves in time. The divergence of the mean squared separation but the convergence of the mean separation however, indicate a densely populated tail in the Boltzmann distribution. This will also be visible in Monte Carlo simulations: long simulation times will be needed to compensate for the effects of the tail.

Finally, simulations on three dimensional network glasses suggest that these materials also show anomalous diffusive behavior [17]. Applying this method in three dimensions might lead to better understanding of the viscosity in glasses. Also, for three dimensional glasses often the Keating parameters α_K and β_K are known from measurements. This could lead to for instance physical critical temperatures that should be experimentally verifiable. For graphene this is not yet the case, since these parameters are unknown so far.

6 Conclusion

Structural defects in graphene have found to be crucial for the understanding of the mechanics of graphene. First, the ground state of graphene has been explored by considering carbon atoms and their ability to form bonds with one another. The result was a regular hexagonal lattice. The Keating potential was used since this potential both yields the correct ground state and is computable even for large systems. Excitations of the ground state were considered, under the conditions that the number of atoms remain invariable and that the energy of the defect should be finite. A Stone-Wales defect in an otherwise perfect lattice was observed to be the energetically favorable excitation. The two pentagon-heptagon pairs that form such a defect were able to move in the zigzag direction without affecting the number of defects, thus defining the state space of the system.

States of defected graphene were then defined in terms of the defect separation in the zigzag direction. The presence of defects was observed to deform the lattice. The energies of these states were minimized according to the Keating potential and equilibrium energies and deformation were calculated in terms of the separation. Using the energies, the partition function, mean separation and mean squared separation were computed. This resulted in three regimes: one where both the mean separation and the mean squared separation diverge, one where the first converges and the second diverges and one where both converge.

After studying equilibrium properties of defected graphene, the system's behavior in time was considered. The defect separation was observed to be able to increase or decrease one step at the time. In order to do this, the lattice had to both rearrange bonds to create a new topology and reposition atoms to minimize energy in the new state. This was modeled by an energy barrier between consecutive equilibrium states. The transition probabilities were modeled according to a stochastic process. A matrix containing probabilities to move from a state with separation i to another state with separation j in some time t was computed for all states i and j and for all times t.

Using this matrix, the mean squared displacement of the separation was calculated as a function of time at different temperatures. This yielded two regimes: one in which the mean squared displacement showed subdiffusive behavior and one in which it converged to a constant. In between these regimes, at a critical temperature, the mean square displacement was observed to diverge logarithmically. Applying Einstein-Smoluchowski to this system led to a relation for the shear deformation of defected graphene in time. Graphene was calculated to shear infinitely as a result of a small external stress, but with a non-constant shear velocity. This shear velocity decreased over time and eventually became zero even though the shear itself increased to infinity.

Research on three dimensional network glasses suggests that they too exhibit anomalous diffusion. Applying this method in three dimensions might lead to more understanding of this behavior. It is important to then also consider the interactions between multiple defect pairs and to explore whether Einstein-Smoluchowski is still valid for these kind of non-Brownian particles. If the correct parameters of the Keating potential are known, the effects found should be experimentally verifiable.

References

[1] Geim A. K., 2009, Graphene: status and prospects, *Science* **324** 1530

[2] Novoselov, K. S., Geim, A. K., Morozov, S. V., Jiang, D., Zhang, Y., Dubonos, S. V., Gregorieva I. V., and Firsov, A. A., 2004, *Science* **306** 666

[3] Kittel, C., 2005, *Introduction to Solid State Physics*, John Wiley & Sons: New York

[4] Mermin, N. D., 1968, Crystalline Order in Two Dimensions, *Phys. Rev.* **176** 250.

[5] Hashimoto, A., Suenaga, K., Gloter, A., Urita, K. and Iijima, S., 2004, Direct Evidence for Atomic Defects in Graphene Layers *Nature* **430** 870.

[6] Gass, M. H., Bangert, U., Bleloch, A. L., Wang, P., Nair, R. R. and Geim, A. K., 2008, Free-Standing Graphene at Atomic Resolution, *Nat. Nanotechnol.* **3** 676.

[7] Meyer, J. C., Kisielowski, C., Erni, R., Rossell, M. D., Crommie, M. F. and Zettl, A., 2008, Direct Imaging of Lattice Atoms and Topological Defects in Graphene Membranes *Nano Lett.* **8** 3582.

[8] Girit, Ç. O., Meyer, J. C., Erni, R., Rossell, M. D., Kisielowski, C., Yang, L., Park, C. H., Crommie, M. F., Cohen, M. L., Louie, S. G., et al., 2009, Graphene at the Edge: Stability and Dynamics *Science* **323** 1705

[9] Keating, P. N., 1966, Effect of Invariance Requirements on the Elastic Strain Energy of Crystals with Application to the Diamond Structure, *Phys. Rev.* **145** 637

[10] Alben, R., Smith, J.E., Brodsky, M. H. and Weaire, D., 1973, Theory of Infrared and Raman Spectra of Amorphous Si and Ge, *Phys. Rev. Lett.* **30** 1141

[11] Wooten, F. and Weaire, D., 1987, Modeling Tetrahedrally Bonded Random Networks by Computer, *Solid State Physics* **40** 1

[12] Kumar, A., Wilson, M. and Thorpe, M. F., 2012, Amorphous graphene: a realization of Zachariasen's glass, *Condens. matter* **24** 485003

[13] Ross, S. M., 2009, *Introduction to Probability Models*, Elsevier Science Publishing

[14] Einstein, A., 1905, ber die von der molekularkinetischen Theorie der Wrme geforderte Bewegung von in ruhenden Flssigkeiten suspendierten Teilchen, *Annalen der Physik* **322** 549

[15] von Smoluchowski, M., 1906, Zur kinetischen Theorie der Brownschen Molekularbewegung und der Suspensionen, *Annalen der Physik* **326** 756

[16] Ferrari, P. A., 1986, The simple exclusion process as seen from a tagged particle, *The Annals of Probability*, **14** 1277

[17] Dilz, R. J., 2011, Anomalous dynamics in a glassy material around its glass transition, MSc. thesis, Utrecht University